SAND2015-5557C

Addressing Angular Single-Event Effects in the Estimation of On-Orbit Error Rates

David S. Lee, *Graduate Student Member, IEEE*, Gary M. Swift, *Member, IEEE,* and Michael J. Wirthlin, *Senior Member, IEEE*

***Abstract*—This study describes complications introduced by angular direct ionization events on space error rate predictions, proposes a methodology to extend existing error estimation, and illustrates these points using test data on a modern 28nm device.**

***Index Terms*—Radiation effects, single event effects, multiple bit upset, multiple cell upset.**

I. Introduction

Estimating the error rate for space electronics is extremely important to spacecraft designers. As technology scales shrink, producing accurate on-orbit error rate estimates is becoming increasingly difficult due to changes in error signatures [1]. In particular, heavy-ion events have increasing multiple-cell upset (MCU) rates due to charge sharing [2]. In addition, rotational variations are becoming more prominent, violating the concept of effective linear energy transfer (LET). In order to properly predict space rates for leading-edge and emerging technologies, routine single-event effects testing needs take additional data to support modified calculation-based models that include consideration of angular error signatures.

This study examines the effect of angular direct ionization events on space event rate estimates and proposes a method to apply existing single-bit single-event upset (SEU) models to both existing and new technologies. Testing methodology for a 28 nm SRAM-based device is presented and illustrates the technique applied which extends existing single-event rate prediction models to account for angular ionization events encountered in orbit.

Submitted for review on July 10, 2015. This work was supported by the Laboratory Directed Research and Development program at Sandia National Laboratories, a multi-program laboratory managed and operated by Sandia Corporation, a wholly owned subsidiary of Lockheed Martin Corporation, for the U.S. Department of Energy's National Nuclear Security Administration under contract DE-AC04-94AL85000 and by the I/UCRC Program of the National Science Foundation under Grant No. 1265957. Unclassified, unlimited release under SAND2015-XXXX. All trademarks, service marks, and trade names are the property of their respective owners.

D. S. Lee is with Sandia National Laboratories, Albuquerque, NM 87123 USA. (e-mail: dslee@sandia.gov)

G. Swift is with Swift Engineering & Radiation Services, LLC, San Jose, CA 95124 USA (e-mail: gary@swiftradiation.com).

M. Wirthlin is with the Center for High Performance Reconfigurable Computing, Brigham Young University, Department of Electrical and Computer Engineering, Provo, UT 84602 USA (e-mail: wirthlin@byu.edu).

II. Difficulties in Rate Prediction

A significant breakdown of existing rate prediction models relates to the consideration of ion strikes that occur at angles other than normal incidence. In particular, there are two problems that result from a dependence on rotation angle when ions strike the device with a non-zero tilt angle: the use of "effective LET" and the generation of MCUs. These factors affect the accuracy of current on-orbit rate prediction models.

The nomenclature in this paper will define an event as a single ion striking a sensitive volume that causes one or more cells to upset. A bit upset is defined as a single memory bit that changes state from an event. One event may cause a MCU, which is the collection of bit upsets from a single event. In order to provide orientation for ions striking the device, Fig. 1 defines the orientation for tilt (Θ_T) and rotation (Θ_R) to define the direction of incidence.

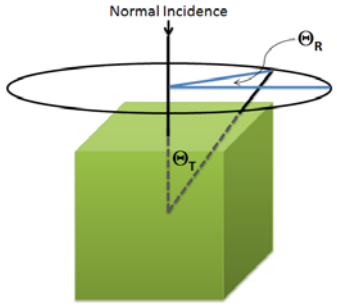

Fig. 1. Orientation of tilt (Θ_T) and rotation (Θ_R) for ion strikes into a sensitive volume of silicon.

A. Effective LET

Effective LET, defined as the incident LET divided by the cosine of the tilt angle, has served the radiation effects community well for decades as a key simplifying concept (along with "critical charge" to upset). However, the "cosine law" works best for thin pancake shaped charge collection volumes that are widely separated and at least several ion track diameters apart so that charge sharing is negligible; neither assumption is true at current scale. Thus, it is not surprising to see test data with serious cosine law breakdowns and simulation studies that explain why in detail. At least one replacement "law" [3] and at least one complete replacement rate method [4] have been developed, but are too complicated for wide adoption to date.

Data from this work's exemplar, the 28 nm Kintex-7 Field Programmable Gate Array (FPGA), demonstrates these

breakdowns in Fig. 2, which shows a variety of rotations for several discrete tilt angles. The graph illustrates the range of cross-sections that can be experimentally obtained when attempting to utilize the cosine law to establish higher effective LET by increasing Θ_T. Although Θ_T is an important variable, it can be clearly seen that consideration must be given to Θ_R as well, especially if tilting at higher angles above 60 degrees.

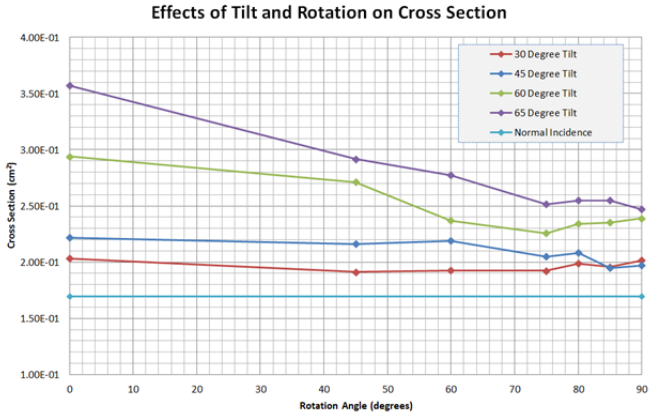

Fig. 2. The rotation angle dependence of the cross section of a 28 nm SRAM device for several tilt angles violates the inherent "effective LET" assumption that tilt angle is the only variable. This data is obtained with Kr at a nominal LET of 26.4 [MeV-cm^2/mg].

The strong rotational dependence of Fig. 2 can be from either differences in row vs. column spacing or may be due to well orientation [5]; regardless, it is apparently a growing problem as node size scales. Industry-standard rate calculators like SPENVIS [6] and CREME96 [7] cannot deal with this effect because rotation angle independence is built into the models.

B. Multiple-Cell Upsets

The other problem related to rotational dependence is the generation of MCUs. Through data obtained from irradiation of the 28 nm SRAM FPGA memory array [8, 9], generation of MCU events has been observed at relatively low LET thresholds and has become a non-trivial factor when considering bit upset counts. It is well known that higher MCU rates arise from shrinking node sizes due to increased charge sharing [1, 10-12]. As a practical matter, the varying shape and bit count of MCU patterns make it difficult to isolate the events that caused these upsets – a non-trivial issue for rate prediction [13].

The problem of MCU generation is also aggravated by a rotational dependence that exists with respect to the orientation of SRAM cells within the device. For example, the Kintex-7 SRAM cells are arranged such that memory words span down columns with spacing between groups of logically adjacent words. Because of well sharing, cell-to-cell proximity, and their columnar organization, non-normal-incident ions that strike along the columns (near Θ_R=0° for Θ_T>0°) create significantly higher MCU sizes than those that strike against the columns (near Θ_R=90° for Θ_T>0°). Fig. 3 illustrates this principle.

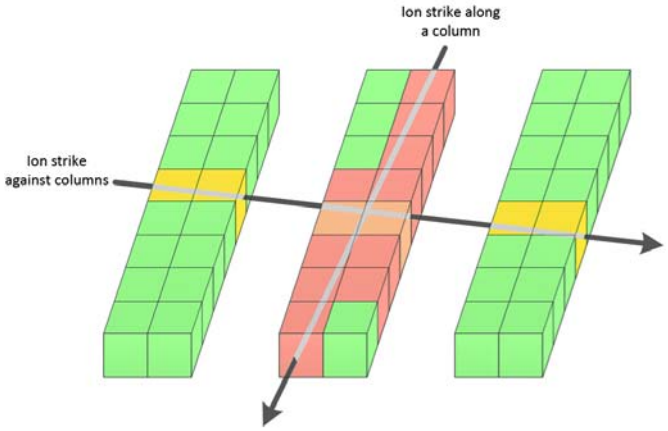

Fig. 3. Layout characteristics can cause a dependence on Θ_R for ion strikes when $\Theta_T > 0$. The organization of the SRAM cells in the device above will upset a significantly higher number of cells when ions strike along columns, rather than against them.

As a case study, the ratio of MCUs compared to single bit upsets (SBU) was examined for the experimental data obtained on Kintex-7. Fig. 4 shows the graphical representation of relative MCU generation and its dependence on Θ_R and Θ_T. Due to the physical organization of the SRAM cells, both the incidence and size of MCU events is higher when ions strike along the columns, compared to striking against the columns or at normal incidence.

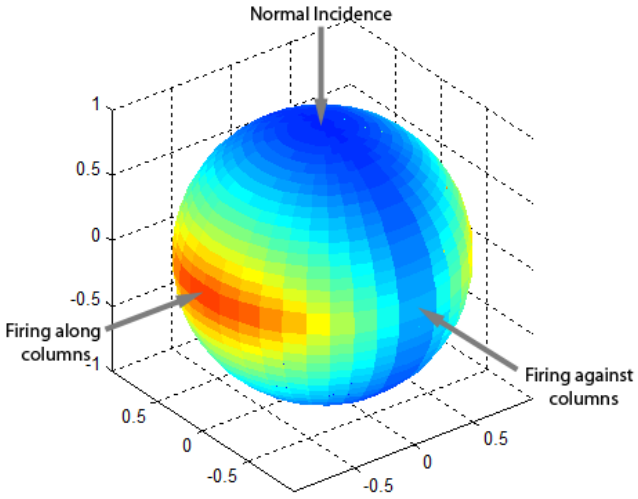

Fig. 4. An illustration of the relative MCU prevalence with respect to tilt and rotation. Ions striking parallel to the columns will substantially increase the likelihood of MCU generation compared to ion strikes.

Existing rate estimation models generally analyze only individual sensitive volumes and do not consider neighboring sensitive volumes or the presence of MCU. Even if models were to consider adjacent sensitive volumes, the fact that each node collects a different portion of liberated charge makes this model problematic when charge sharing is involved as a mechanism of upset [14].

When considering angular data, existing models will over-estimate the on-orbit rate since angular strikes can have significantly higher MCU rates which inflate raw bit upset

counts – the foundation for rate prediction. This is also a problem in modern devices which are showing rising MCU rates even when ions strike at normal incidence.

Rather than generate new, inevitably complex models that factor in rotational angles and MCU statistics, a methodology is proposed in the following section which is able to utilize existing single-bit upset (SBU) models to obtain error rates using data consistent with existing collection methods and techniques.

III. Methodology

In order to effectively utilize existing on-orbit rate prediction models, both MCU clusters and rotational dependence must first be addressed. Current testing techniques for memory-based technologies typically evaluate upset rate as a function of LET and the number of bits that are upset in the device following an experimental irradiation. The methodology proposed will address the conversion of this data obtained from standard SEE testing practices in order to extract event rates (where one event equates to one ion striking the device), then modulate the data based on the MCU response of the device at all potential rotation and tilt angles.

It is important to note that some symmetry in the device construction is necessary in order for this method to be effective. Fortunately, this will be the case for most devices, but there may be some rare instances where specific device construction prohibits the use of assumptions made in the methodology.

A. Experimental Data Collection

In order to address rotational dependence, a certain amount of accelerator testing at various tilt and rotation angles is necessary. The data from testing at these angles should reduce observed bit errors into event counts as discussed in the prior section. The problem that arises in attempting to experimentally identify angular MCU rates is the relatively large test matrix needed, comprised of a permutation of possible rotations and tilt combinations ($0° \leq \Theta_R < 360°$, $0° \leq \Theta_T < 360°$). Since testing at every combination of rotation and tilt is not feasible, the required test space has to be reduced in order to be tractable. Taking advantage of symmetries turns out to be quite effective in reducing the test matrix to a reasonable size.

There are two assumptions that need to be made in order for this reduction method to apply. First, it is assumed that the sensitive volume is cuboid-shaped (rectangular faces joined by right angles). In order to provide orientation for the remainder of this discussion, any ion entering at $\Theta_T=0°$ will be considered to strike the volume at normal incidence from the top face of the cuboid. An ion entering from $\Theta_T=90°$, $\Theta_R=0°$ shall be normally incident to either of the side faces.

The second assumption this method will make is that two ions that traverse the same path through a sensitive volume will have the same net effect, even if the ions are traveling in opposite directions having entered from opposite sides of the sensitive volume. Thus, an ion traveling through the sensitive volume at $\Theta_T=90°$, $\Theta_R=0°$ will have the same path and present the same cross-section as an ion at $\Theta_T=90°$, $\Theta_R=180°$, despite the fact they are traveling in opposite directions.

For general device layouts, these assumptions mean that the cross-section "seen" by an ion for $0° \leq \Theta_R < 90°$ at any given Θ_T should be equal to that for $180° \leq \Theta_R < 270°$, and should be symmetric for cases of $90° \leq \Theta_R < 180°$ and $270° \leq \Theta_R < 360°$. Thus, by testing at rotations of $0° \leq \Theta_R < 90°$, data can be obtained that will apply for $90° \leq \Theta_R < 360°$, reducing the required test matrix by a factor of four. Furthermore, by the same principle, ions traveling in exactly opposite directions with respect to tilt should be considered equal (that is, where $\Theta_T' = \Theta_T + 180°$). This again reduces the test matrix by half.

The net result is an eight-fold reduction of the required testing space, as indicated by the yellow section in Fig. 5.

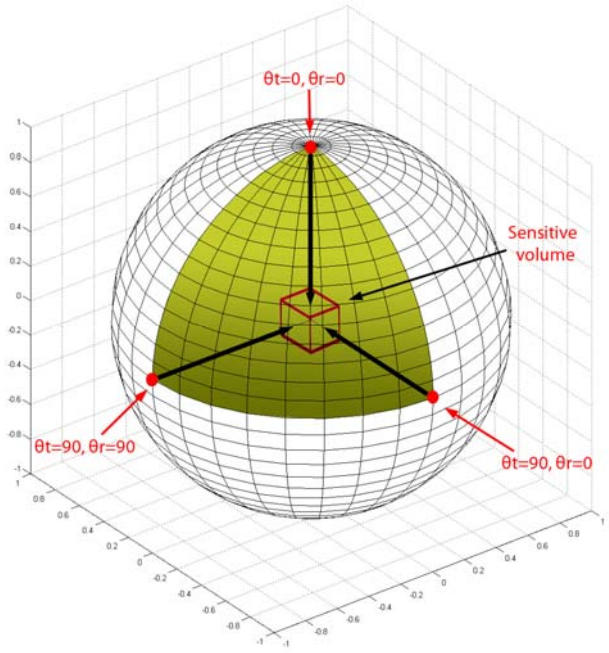

Fig. 5. Reduced test matrix after consideration of symmetry. The wedge can be symmetrically translated to the other three quadrants in the top hemisphere. Furthermore, the entire top hemisphere is symmetric to the bottom hemisphere.

The cross-section for all points within the yellow wedge (bounded by the three points above) would ideally be obtained experimentally. However, as mentioned before, the extremely large matrix of possible rotation and tilt combinations (even for this reduced angle set) makes this unreasonable to attempt. The most important points, which we will refer to as the "boundary points," are at $(\Theta_R, \Theta_T) = (0°,0°)$, $(0°, 90°)$, and $(90°, 90°)$ which provide the relative contribution from ions incident on each face of the sensitive volume. From there, we can attempt to interpolate data for points within the yellow wedge in Fig. 5 using the boundary points.

A potential problem, though, is the inability to obtain data at $\Theta_T=90°$, due to the limitations on available cyclotron ion range, obstruction of other board components, and so forth. To solve this issue, key data points with respect to rotation and tilt should be obtained which can then be used to extrapolate missing data at $\Theta_T=90°$. Those points should be along the line from normal incidence approaching $\Theta_T=90°$ for both $\Theta_R=0°$ and $\Theta_R=90°$ (also depicted by the "edges" of the yellow wedge

originating from the top pole of the sphere in Fig. 5). As many tilt angles as reasonably possible should be obtained for these two rotations, and to as steep a tilt angle as ion penetration will allow.

B. Conversion to Event Rates

In order to address the MCU problem, this proposed methodology seeks to further refine the data observed through accelerator testing to distinguish between the number of events and the number of upset bits. Regardless of the distribution of MCU cluster sizes, the event rate is the important factor that should be assessed, not the bit upset rate (which is always higher due to MCUs). This behavior will allow us to utilize standard event rate estimation tools which typically assume that one ion striking the device will cause one bit to upset; by modifying the data set to evaluate MCU event rate instead of upset bit count, the tools will be able to provide a proper one-to-one mapping of ion strikes to events in the device.

In order to break down data obtained from accelerator testing (bit upset rate) into an event rate, the data from accelerator tests must be examined in order to see which bits in the device have upset. Clusters of upset bits that are physically adjacent should be grouped together into one event.

A considerable challenge when attempting to obtain MCU events is that the physical layout of the device is typically not known. Also, techniques such as physical interleaving of memory words can cause physically adjacent bits on the die to be logically mapped into different words in the address space that are presented to the end-user, thus obscuring the boundaries between adjacent bits.

One method to identify which bits are physically adjacent when the exact layout and physical-to-logical address mapping is not known is to utilize the method described in [8]. This method identifies physically adjacent cells through statistical probability and is able to estimate which bits in error may in fact be physically adjacent on the die and thus in a MCU cluster, even if they are not adjacent in the device's memory space. This addresses one of the significant problems identified in [13] with respect to error rate prediction in the presence of MCUs.

It is important to ensure that when collecting experimental data, the number of upset bits should be very small relative to the total number of bits in the device. Although it is improbable that two SBU events will cause a "coincident SBU" (two distinct single-bit upset events that are physically adjacent and appear as a MCU), it is important to keep the event count low for each irradiation as to minimize the probability of SBU occurrences.

C. Extrapolating and Interpolating Missing Data

As mentioned earlier, it is generally not possible to obtain experimental data at the three boundary conditions because of the physical limitations that prevent data collection at Θ_T=90. However, the data obtained obtained in section A from varying Θ_T can be fit through a fitting function in order to extrapolate the data out to obtain an approximation for Θ_T=90 in both the Θ_R=0 and Θ_R=90 cases. A cosine-based fit seems to work well with experimental data analyzed to date.

Let us first examine the case where Θ_R=0°. To perform extrapolation for Θ_R=0°, Θ_T=90°, we first make a guess at the cross-section at that point.

Using a cosine shape, we then interpolate data points weighted between the experimentally-obtained cross-section at normal incidence and our guess of the cross-section at Θ_R=0°, Θ_T=90°. The equation for interpolation of data points between 0- and 90-degree tilt data points is given below in Eqn. 1. For the parameters in Eqn 1., σ_{90} is our guess at the cross-section, σ_0 is experimentally-obtained normal incidence cross-section data, σ_n represents the interpolated cross-section at angle n-degrees, and S_n is a weighting factor that gives the interpolated values a cosine "shape." To obtain the interpolated cross-section σ_n, weighted contributions from σ_0 and σ_{90} (where the weight is determined by the cosine function S_n) are summed to form the interpolated value.

Let:
σ_0 = *Cross-section at 0-degree tilt (normal incidence)*
σ_{90} = *Cross-section at 90-degree tilt*
σ_n = *Cross-section at n-degree tilt*
Z_n = *Tilt angle at n degrees*
S_n = *Weighting factor equal to* $\frac{\cos(2*Z_n)+1}{2}$

Then values may be interpolated by:

$$\sigma_n = [(\sigma_0 * S_n) - \sigma_{90} * (1 - S_n)]. \quad (1)$$

Once values are interpolated between a tilt of 0 and 90 degrees, the interpolated values can then be compared to the experimentally obtained data at tilt angles for which we have experimental data when Θ_R=0°. We can obtain the error using a least-squares fit comparing the extrapolated data points to the experimentally obtained data, for any tested Θ_T data points at Θ_R=0°. The error is given by Eqn. 2 below:

Let:
E = *Fitting error*
$\sigma_{0..n}$ = *Experimentally obtained cross-sections for tilt angles at a fixed rotation*
$\sigma'_{0..n}$ = *Interpolated cross-section corresponding to experimentally obtained angles*

$$\sum_{i=0}^{n} (\sigma_i - \sigma'_i)^2 = E. \quad (2)$$

The process of guessing σ_{90} is iterative and should be repeated with the goal of minimizing E (or ideally pushing it to zero). Once a good fit is found for the Θ_R=0° case, the same process can be repeated with the data at Θ_R=90° to extrapolate the data at Θ_R=90°, Θ_T=90°.

Once the boundary points are found, the process in Eqn. 1 can be repeated to interpolate the remaining data points, not only for the lines connecting boundary points, but for intermediate points away from the edges of the yellow wedge in Fig. 5.

This accuracy of this process depends on the number of actual experimental data points that can be obtained. Especially for the initial data set used to interpolate the

Θ_T=90° values, time constraints will dictate a maximum number of angle combinations that can be tested. It is important to select tilt and rotation combinations when obtaining the data in step A such that data points are spaced apart as much as possible. Thus, in selecting angles to test and when not limited by some other factor, it is important that the selected angles for tilt and rotation should not be evenly distributed from 0° to 90°, but rather should be distributed the based on function of the cosine of Θ.

Let us first examine a method to determine test angles for rotation (the same concepts extend to determining tilt angles as well). Since we assume that the case of Θ_R=Θ_R+180°, a cosine plot with a period of 180° is used as shown below in Fig. 6. The red points indicate the three most important rotations. The first point at Θ_R=0 will provide data for ions normally incident to one face of the sensitive volume. The third point at Θ_R=90 provides data for normal incidence to the adjacent face. The point on the curve halfway in between is represented by the second red point at Θ_R=45. If further subdivision is desired, the angle where the cosine yields half the distance between existing points should be selected. Thus, the next subdivision, represented by the green points, occurs at Θ_R=30° and Θ_R=60°. If even more points are desired, subdividing further yields angles of Θ_R={22.5°, 37.5°, 52.5°, 67.5°} (shown as blue points).

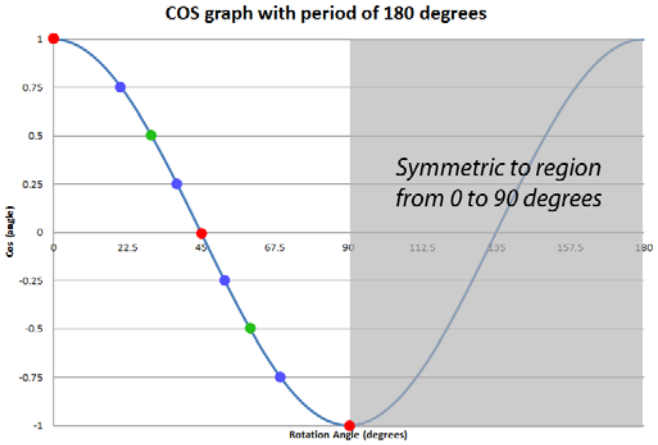

Fig. 6. When selecting rotation angles to test, it is important to not divide the test angles evenly across the test range; rather a cosine-based division is preferred to ensure data is spread out evenly. Red represents first choice for angles to test, followed by green and lastly blue.

D. Averaging of Interpolated Data

Once data is obtained for the full range of angles on both tilt and rotation, the interpolated data should provide a matrix of cross-section at any given angle combination of rotation and tilt. The average of all of these values should be taken and this average cross-section should replace the data point for the cross-section at this particular ion's incident LET. By averaging all of the cross-section numbers together, the data is made rotationally independent to match the models used by industry standard tools.

This procedure is then repeated for the remaining test LETs and ultimately produces a cross-section curve averaging all rotational effects and representing only event rates. This cross-section can then be used in existing single-bit single-event on-orbit rate prediction models to get an on-orbit rate with increased accuracy.

IV. Case Study

As a demonstration of this methodology, this work examined the irradiation of a Xilinx Kintex-7 XC7V325T FPGA, which is fabricated on a modern 28 nm TSMC process. The configuration memory of the Kintex-7 is comprised of a SRAM memory array with 72,868,672 bits. The device was irradiated with heavy ions at Lawrence Berkeley Laboratory's 88-inch Cyclotron in September of 2014.

The test procedure would initialize the FPGA configuration memory array, begin irradiation, and stop irradiation once a certain threshold of errors was reached. Readback of the SRAM memory array occurred every 10 seconds at low flux, in order to minimize the chance of coincident SBU, where a pair of single-bit upsets would mimic a MCU signature. This also enables ready filtering of control circuit upsets that cause large apparent "bursts" of bit upsets.

In order to obtain the requisite data to analyze the effect of MCUs on the space rate for this particular device, part irradiation was performed at 0- (normal), 50-, 60-, and 70-degree tilt. Following this, the part was rotated 90 degrees and irradiation performed at 50-, 60-, and 70-degree tilt. 70 degrees was the practical limit of tilt for the test board used. The data counts are presented below in Table 1.

Table 1. Raw data from Kintex-7 study.

Ion	Incident LET	Tilt	Rotation	Fluence	Events	Bits upset	Event Cross-Section	Bit Cross-Section
O	1.54	0	0	1.99E+06	18400	18681	9.23E-03	9.37E-03
O	1.54	50	0	1.58E+06	19798	21892	1.25E-02	1.39E-02
O	1.54	60	0	1.35E+06	20178	24282	1.49E-02	1.80E-02
O	1.54	70	0	1.11E+06	18364	26371	1.65E-02	2.38E-02
O	1.54	50	90	4.78E+06	21328	22226	4.46E-03	4.65E-03
O	1.54	60	90	5.86E+06	20372	21666	3.47E-03	3.70E-03
O	1.54	70	90	6.33E+06	20171	21829	3.19E-03	3.45E-03
Si	4.35	0	0	6.25E+05	19643	22067	3.14E-02	3.53E-02
Si	4.35	50	0	1.09E+05	5481	6999	5.01E-02	6.40E-02
Si	4.35	60	0	1.09E+05	4787	7203	4.39E-02	6.61E-02
Si	4.35	70	0	1.14E+05	4837	8735	4.25E-02	7.68E-02
Si	4.35	50	90	1.20E+05	5728	6584	4.78E-02	5.50E-02
Si	4.35	60	90	1.29E+05	6043	7056	4.70E-02	5.49E-02
Si	4.35	70	90	1.50E+05	5616	6923	3.73E-02	4.60E-02
Ar	7.27	0	0	3.52E+05	13275	16013	3.77E-02	4.55E-02
Ar	7.27	50	0	3.27E+05	14979	20979	4.59E-02	6.42E-02
Ar	7.27	60	0	3.41E+05	14591	24438	4.28E-02	7.17E-02
Ar	7.27	70	0	3.17E+05	6288	12406	1.98E-02	3.91E-02
Ar	7.27	50	90	3.16E+05	15314	18636	4.85E-02	5.91E-02
Ar	7.27	60	90	3.02E+05	16827	21309	5.57E-02	7.05E-02
Ar	7.27	70	90	2.63E+05	14283	18735	5.43E-02	7.13E-02
Xe	49.3	0	0	2.08E+05	41230	66293	1.98E-01	3.18E-01
Xe	49.3	45	0	6.78E+04	13635	25308	2.01E-01	3.73E-01
Xe	49.3	50	0	6.50E+04	15241	29878	2.35E-01	4.60E-01
Xe	49.3	45	90	8.07E+04	18614	31168	2.31E-01	3.86E-01
Xe	49.3	50	90	5.60E+04	11790	20105	2.10E-01	3.59E-01
Xe	49.3	55	90	8.00E+04	19006	33585	2.38E-01	4.20E-01

The irradiations were performed using ion species and energies such that the incident LETs were 1.54, 4.35, 7.27, and 49.3 [MeV-cm^2/mg]. For each ion, data was extrapolated using Eqn. 1 and 2 described earlier in this paper to obtain steeper than 70-degree tilt points for each available rotation. The data remaining data was then interpolated between 0 and

Table 2. Start of interpolation process for Oxygen event rate data. The first step is to extrapolate the 90-degree tilt values for rotations where we have experimental data. The remainder of the unknown values for each row is then interpolated using the cosine fit. The light green locations represent actual data.

Rotation \ Tilt	0	5	10	15	20	25	30	35	40	45	50	55	60	65	70	75	80	85	90
0	1.27E-10	1.32E-10	1.46E-10	1.69E-10	2.01E-10	2.40E-10	2.86E-10	3.36E-10	3.89E-10	4.44E-10	2.68E-10	5.52E-10	4.10E-10	6.48E-10	6.64E-10	7.19E-10	7.42E-10	7.56E-10	7.61E-10
5																			
10																			
15																			
20																			
25																			
30																			
35																			
40																			
45																			
50																			
55																			
60																			
65																			
70																			
75																			
80																			
85																			
90	1.27E-10	1.27E-10	1.26E-10	1.24E-10	1.22E-10	1.20E-10	1.17E-10	1.13E-10	1.10E-10	1.06E-10	9.52E-11	9.93E-11	9.54E-11	9.31E-11	1.28E-10	8.85E-11	8.69E-11	8.60E-11	8.57E-11

90 degrees of tilt using Eqn. 1. This first step of obtaining boundary points is shown above in Table 2.

Following the complete interpolation along the rows with available data, the data is then interpolated along the columns for each tilt angle, again using Eqn. 1, in order to obtain approximate cross-sections as the device is rotated from 0 to 90 degrees. This is shown at the bottom of the page in Table 3. Using the complete matrix, we can now obtain the average cross-section and use this value in place of the per-bit cross-section for that incident LET.

Following this process for all available data and ions, the change in cross-section can then be evaluated when evaluating event rates to bit upset rates is shown in Fig. 7. The difference in on-orbit error rates is shown in Table 4.

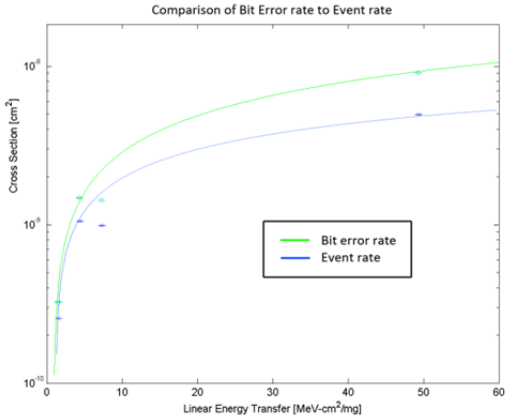

Fig. 7. The difference between the bit error rate and the extracted event error rate is shown here. The event rate should be the parameters used in space error rate estimation tools that are built upon the priciniple that one ion causes only one bit to upset.

Table 4. Predicted on-orbit error rate differences are given when evaluating data by raw bit upset rate versus the actual event rate.

Methodology	Angles	Predicted Errors per device per day	Calculated Difference
Events	All angles considered	3.621	-
Bit rate	All angles considered	6.2	71.22%

V. Conclusion

This work introduces four novel innovations towards solving problems presented by the stronger MCU response of modern scaled technology nodes. First, the methodology for extracting physical layout information presented last year in

Table 3. Complete interpolation of event rate data for Oxygen. Actual data points are shown in light green.

Rotation \ Tilt	0	5	10	15	20	25	30	35	40	45	50	55	60	65	70	75	80	85	90
0	1.27E-10	1.32E-10	1.46E-10	1.69E-10	2.01E-10	2.40E-10	2.86E-10	3.36E-10	3.89E-10	4.44E-10	2.68E-10	5.52E-10	4.10E-10	6.48E-10	6.64E-10	7.19E-10	7.42E-10	7.56E-10	7.61E-10
5	1.27E-10	1.32E-10	1.46E-10	1.69E-10	2.01E-10	2.39E-10	2.84E-10	3.34E-10	3.87E-10	4.41E-10	2.67E-10	5.49E-10	4.08E-10	6.44E-10	6.60E-10	7.14E-10	7.37E-10	7.51E-10	7.56E-10
10	1.27E-10	1.32E-10	1.46E-10	1.68E-10	1.99E-10	2.37E-10	2.80E-10	3.29E-10	3.81E-10	4.34E-10	2.63E-10	5.39E-10	4.01E-10	6.31E-10	6.48E-10	7.00E-10	7.22E-10	7.36E-10	7.41E-10
15	1.27E-10	1.31E-10	1.45E-10	1.66E-10	1.96E-10	2.32E-10	2.74E-10	3.21E-10	3.70E-10	4.21E-10	2.56E-10	5.22E-10	3.89E-10	6.11E-10	6.28E-10	6.76E-10	6.98E-10	7.11E-10	7.16E-10
20	1.27E-10	1.31E-10	1.44E-10	1.64E-10	1.92E-10	2.26E-10	2.66E-10	3.10E-10	3.56E-10	4.05E-10	2.48E-10	4.99E-10	3.73E-10	5.83E-10	6.01E-10	6.45E-10	6.65E-10	6.78E-10	6.82E-10
25	1.27E-10	1.31E-10	1.42E-10	1.61E-10	1.87E-10	2.19E-10	2.55E-10	2.96E-10	3.39E-10	3.84E-10	2.37E-10	4.71E-10	3.54E-10	5.49E-10	5.68E-10	6.06E-10	6.25E-10	6.36E-10	6.40E-10
30	1.27E-10	1.31E-10	1.41E-10	1.58E-10	1.81E-10	2.10E-10	2.43E-10	2.80E-10	3.19E-10	3.60E-10	2.25E-10	4.39E-10	3.31E-10	5.09E-10	5.30E-10	5.61E-10	5.78E-10	5.89E-10	5.92E-10
35	1.27E-10	1.30E-10	1.39E-10	1.55E-10	1.75E-10	2.01E-10	2.30E-10	2.62E-10	2.97E-10	3.33E-10	2.11E-10	4.03E-10	3.06E-10	4.65E-10	4.88E-10	5.11E-10	5.26E-10	5.36E-10	5.39E-10
40	1.27E-10	1.30E-10	1.38E-10	1.51E-10	1.69E-10	1.90E-10	2.16E-10	2.44E-10	2.74E-10	3.04E-10	1.97E-10	3.65E-10	2.80E-10	4.19E-10	4.43E-10	4.58E-10	4.71E-10	4.79E-10	4.82E-10
45	1.27E-10	1.29E-10	1.36E-10	1.47E-10	1.62E-10	1.80E-10	2.01E-10	2.24E-10	2.49E-10	2.75E-10	1.82E-10	3.26E-10	2.53E-10	3.70E-10	3.96E-10	4.03E-10	4.14E-10	4.21E-10	4.23E-10
50	1.27E-10	1.29E-10	1.34E-10	1.43E-10	1.55E-10	1.69E-10	1.86E-10	2.05E-10	2.25E-10	2.46E-10	1.67E-10	2.87E-10	2.25E-10	3.22E-10	3.49E-10	3.49E-10	3.58E-10	3.63E-10	3.65E-10
55	1.27E-10	1.28E-10	1.32E-10	1.39E-10	1.48E-10	1.59E-10	1.72E-10	1.87E-10	2.02E-10	2.17E-10	1.52E-10	2.48E-10	1.99E-10	2.76E-10	3.04E-10	2.96E-10	3.02E-10	3.06E-10	3.08E-10
60	1.27E-10	1.28E-10	1.31E-10	1.36E-10	1.42E-10	1.50E-10	1.59E-10	1.69E-10	1.80E-10	1.91E-10	1.38E-10	2.13E-10	1.74E-10	2.32E-10	2.62E-10	2.46E-10	2.51E-10	2.54E-10	2.55E-10
65	1.27E-10	1.28E-10	1.29E-10	1.32E-10	1.36E-10	1.41E-10	1.47E-10	1.53E-10	1.60E-10	1.67E-10	1.26E-10	1.80E-10	1.52E-10	1.92E-10	2.24E-10	2.01E-10	2.04E-10	2.06E-10	2.06E-10
70	1.27E-10	1.27E-10	1.28E-10	1.30E-10	1.31E-10	1.34E-10	1.36E-10	1.39E-10	1.43E-10	1.46E-10	1.15E-10	1.52E-10	1.32E-10	1.58E-10	1.91E-10	1.62E-10	1.64E-10	1.64E-10	1.65E-10
75	1.27E-10	1.27E-10	1.27E-10	1.27E-10	1.27E-10	1.28E-10	1.28E-10	1.28E-10	1.29E-10	1.29E-10	1.07E-10	1.30E-10	1.16E-10	1.30E-10	1.64E-10	1.31E-10	1.31E-10	1.31E-10	1.31E-10
80	1.27E-10	1.27E-10	1.26E-10	1.26E-10	1.25E-10	1.23E-10	1.22E-10	1.20E-10	1.18E-10	1.17E-10	1.00E-10	1.13E-10	1.05E-10	1.10E-10	1.44E-10	1.07E-10	1.07E-10	1.06E-10	1.06E-10
85	1.27E-10	1.27E-10	1.26E-10	1.25E-10	1.23E-10	1.21E-10	1.18E-10	1.15E-10	1.12E-10	1.09E-10	9.65E-11	1.03E-10	9.78E-11	9.73E-11	1.32E-10	9.33E-11	9.19E-11	9.11E-11	9.08E-11
90	1.27E-10	1.27E-10	1.26E-10	1.24E-10	1.22E-10	1.20E-10	1.17E-10	1.13E-10	1.10E-10	1.06E-10	9.52E-11	9.93E-11	9.54E-11	9.31E-11	1.28E-10	8.85E-11	8.69E-11	8.60E-11	8.57E-11

[7] is extended to non-normal angles. Second, specific experiment recommendations are given for identifying the problem of a strong breakdown of effective LET as the independent measuring parameter (that is, where a strong rotation angle effect on cross-section occurs due to directional charge sharing effects). Third, a computational method was developed for filling out a relatively sparse set of angle measurements to a dense virtual data set. Finally, a method for integrating the device angular response with space environments of interest into a normal space rate prediction is demonstrated. The efficacy of these innovations is demonstrated via a complete example using newly acquired heavy ion data on an advanced commercial FPGA, the Xilinx Kintex-7.

REFERENCES

[1] D. G. Mavis, P. H. Eaton, M. D. Sibley, R. C. Lacoe, E. J. Smith, and K. A. Avery, "Multiple Bit Upsets and Error Mitigation in Ultra-Deep Submicron SRAMS," *Nuclear Science, IEEE Transactions on,* vol. 55, pp. 3288-3294, 2008.

[2] O. A. Amusan, A. F. Witulski, L. W. Massengill, B. L. Bhuva, P. R. Fleming, M. L. Alles*, et al.*, "Charge Collection and Charge Sharing in a 130 nm CMOS Technology," *Nuclear Science, IEEE Transactions on,* vol. 53, pp. 3253-3258, 2006.

[3] L. D. Edmonds, "A method for correcting cosine-law errors in SEU test data," *Nuclear Science, IEEE Transactions on,* vol. 49, pp. 1522-1538, 2002.

[4] R. A. Weller, R. A. Reed, K. M. Warren, M. H. Mendenhall, B. D. Sierawski, R. D. Schrimpf*, et al.*, "General Framework for Single Event Effects Rate Prediction in Microelectronics," *Nuclear Science, IEEE Transactions on,* vol. 56, pp. 3098-3108, 2009.

[5] A. D. Tipton, J. A. Pellish, J. M. Hutson, R. Baumann, X. Deng, A. Marshall*, et al.*, "Device-Orientation Effects on Multiple-Bit Upset in 65 nm SRAMs," *Nuclear Science, IEEE Transactions on,* vol. 55, pp. 2880-2885, 2008.

[6] M. Kruglanski, N. Messios, E. De Donder, E. Gamby, S. Calders, L. Hetey*, et al.*, "Last upgrades and development of the space environment information system (SPENVIS)," in *Radiation and Its Effects on Components and Systems (RADECS), 2009 European Conference on*, 2009, pp. 563-565.

[7] A. J. Tylka, J. H. Adams, P. R. Boberg, B. Brownstein, W. F. Dietrich, E. O. Flueckiger*, et al.*, "CREME96: A Revision of the Cosmic Ray Effects on Micro-Electronics Code," *Nuclear Science, IEEE Transactions on,* vol. 44, pp. 2150-2160, 1997.

[8] M. Wirthlin, D. Lee, G. Swift, and H. Quinn, "A Method and Case Study on Identifying Physically Adjacent Multiple-Cell Upsets Using 28-nm, Interleaved and SECDED-Protected Arrays," *Nuclear Science, IEEE Transactions on,* vol. 61, pp. 3080-3087, 2014.

[9] D. S. Lee, M. Wirthlin, G. Swift, and A. C. Le, "Single-Event Characterization of the 28 nm Xilinx Kintex-7 Field-Programmable Gate Array under Heavy Ion Irradiation," in *Radiation Effects Data Workshop (REDW), 2014 IEEE*, 2014, pp. 1-5.

[10] P. E. Dodd and F. W. Sexton, "Critical charge concepts for CMOS SRAMs," *Nuclear Science, IEEE Transactions on,* vol. 42, pp. 1764-1771, 1995.

[11] H. Quinn, P. Graham, J. Krone, M. Caffrey, and S. Rezgui, "Radiation-induced multi-bit upsets in SRAM-based FPGAs," *Nuclear Science, IEEE Transactions on,* vol. 52, pp. 2455-2461, 2005.

[12] D. F. Heidel, P. W. Marshall, J. A. Pellish, K. P. Rodbell, K. A. LaBel, J. R. Schwank*, et al.*, "Single-Event Upsets and Multiple-Bit Upsets on a 45 nm SOI SRAM," *Nuclear Science, IEEE Transactions on,* vol. 56, pp. 3499-3504, 2009.

[13] J. D. Black, P. E. Dodd, and K. M. Warren, "Physics of Multiple-Node Charge Collection and Impacts on Single-Event Characterization and Soft Error Rate Prediction," *Nuclear Science, IEEE Transactions on,* vol. 60, pp. 1836-1851, 2013.

[14] L. D. Edmonds, "Estimates of SEU rates from heavy ions in devices exhibiting dual-node susceptibility," Jet Propulsion Laboratory, National Aeronautics and Space Administration09/19/2011 2011.